Applied Radiation and Isotopes 97 (2015) 118–124

Contents lists available at ScienceDirect

Applied Radiation and Isotopes

journal homepage: www.elsevier.com/locate/apradiso

Temperature effect of a radioluminescent nuclear battery based on ^{147}Pm/ZnS:Cu/GaAs

Xiao-Bin Tang [a,b,*], Liang Hong [a,b], Zhi-Heng Xu [a,b], Yun-Peng Liu [a,b], Da Chen [a,b]

[a] Department of Nuclear Science and Engineering, Nanjing University of Aeronautics and Astronautics, Nanjing 210016, China
[b] Jiangsu Key Laboratory of Material and Technology for Energy Conversion, China

HIGHLIGHTS

- A radioluminescent nuclear battery based on ^{147}Pm/ZnS:Cu/GaAs is presented.
- Electrical performance was measured and calculated at temperature of 223.15–323.15 K.
- Experimental and theoretical values of *Voc* temperature dependence is linear.
- Temperature dependency of semiconductor parameters influences the battery's performance.

ARTICLE INFO

Article history:
Received 11 November 2014
Received in revised form
18 December 2014
Accepted 23 December 2014
Available online 24 December 2014

Keywords:
Radioluminescence effect
Nuclear battery
Temperature effect
Equivalent circuit

ABSTRACT

A radioluminescent nuclear battery was fabricated and the performance was measured and calculated at temperature of 223.15–323.15 K. Experimental and theoretical results indicate that J_{sc} minimally decreases with the increase in temperature, whereas V_{oc} linearly decreases. P_{max} rapidly decreases with temperature. The mechanism of temperature effect is discussed using the temperature dependency of semiconductor parameters. This study significantly guides the selection of batteries' power source under various temperature. The nuclear battery may also be used as a long-life temperature transducer.

1. Introduction

A power supply should have small volume and high energy density because of the miniaturization of microelectromechanical systems (MEMS). A micronuclear battery with long lifetime and high power density can be used as power supply of MEMS in the future (Qiao et al., 2011). Among the numerous competing types of nuclear microbatteries, radioluminescent nuclear batteries exhibit distinct advantages, such as using high-energy charged particles without causing irradiation damage on sensitive photovoltaic cells (Cress et al., 2008; Prelas et al., 2014). A radioluminescent nuclear battery converts the kinetic energy of the particles to fluorescence by using a phosphor material and then to electricity via a photovoltaic cell. This process is an indirect conversion, in which decay energy is converted to fluorescence and then to electricity. A radioluminescent nuclear battery consists of a ^{147}Pm radioactive isotope, ZnS:Cu phosphor layer, and GaAs photovoltaic cell as shown in Fig. 1. The semiconductor materials of the photovoltaic cells significantly affect the battery's performance. The developments in photovoltaic materials and technology have facilitated the use of III–V photovoltaic cells (GaAs, GaP, and related compounds) and solid solutions (AlGaAs, GaInP, and AlGaP) with direct bandgap structures, high light absorption coefficient, and low leakage current in research on radioluminescent nuclear batteries (Bower et al., 2002). Sychov et al. (2008) fabricated a ^{238}Pu/ZnS/AlGaAs indirect conversion radioisotope battery with 21 μW power output. Prelas et al., (1993,1995) produced optoelectronic betavoltaic cells with ^{85}Kr as the radioactive source, luminophor, and wide bandgap photovoltaic cell for absorbing high-energy photon to generate current. Walko et al. (1990) designed radioluminescent photoelectric power sources and indicated that the III–V photovoltaic cell design can generate a power system with smaller volume. Sims et al. (1994) reported the power conversion of ZnS:Ag blue light to electricity for GaP photovoltaic cells.

* Corresponding author at: Department of Nuclear Science and Engineering, Nanjing University of Aeronautics and Astronautics, Nanjing 210016, China. Fax: +86 25 52112906 80407.
E-mail address: tangxiaobin@nuaa.edu.cn (X.-B. Tang).

http://dx.doi.org/10.1016/j.apradiso.2014.12.021
0969-8043/

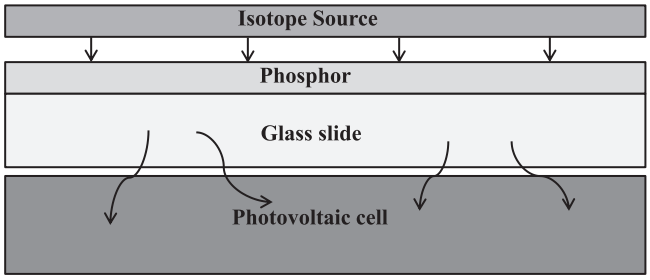

Fig. 1. Schematic of the radioluminescent nuclear battery.

A nuclear battery can be used under extreme conditions, such as in outer space (Brown, 2008) and deep sea, because of its exceptional advantages. These fields are under high- or low-temperature condition, and the temperature varies over a wide range; hence, the electrical performance of a nuclear battery should be examined under different temperatures. For a radioluminescent nuclear battery, the process of the radioactive isotope is not affected by the surrounding temperature; the temperature change slightly the spectral irradiance of the phosphor layer. However, the properties of the photovoltaic cell are easily affected by the temperature.

This paper presents a radioluminescent nuclear battery based on ^{147}Pm/ZnS:Cu/GaAs and determines the temperature effect of the nuclear battery. The temperature was tested from 223.15 K to 323.15 K. The temperature dependency of the bandgap (E_g), depletion-layer widths (w_p and w_n), and intrinsic carrier concentration (n_i) of the semiconductor material are the main factors that theoretically change the electrical performance of the nuclear cell. The theoretical values of the electrical performance were also calculated. The obtained trends were accordingly matched with the experimental results; however, the theoretical values differ because of the existence of series and shunt resistances.

2. Experiment

Some experimental studies on temperature effect of nuclear battery have been carried by investigators recently. Liu et al. (2014) simulated and tested the open-circuit voltage (V_{oc}) and short-circuit current (I_{sc}) of a betavoltaic cell based on ^{63}Ni/Si as a function of temperature; their study concluded that V_{oc} becomes highly sensitive to temperature, and the temperature dependence of V_{oc} can be expressed as an exponential function. Wang et al. (2010) studied the relationship between temperature and electrical performance of two betavoltaic cells; the changing values of V_{oc} within the range of 233.15 K to 333.15 K are −3.1 and −3.0 mV/K, respectively. Moreover, Chandrashekhar et al. (2007) investigated a 4H SiC betavoltaic-powered temperature transducer and obtained a linear sensitivity of 2.7 mV/K.

2.1. Sample preparation

A phosphor layer functions as an energy conversion unit to convert the kinetic energy of decay particles into fluorescence. The raw material and the thickness of the phosphor layer significantly affect the spectral irradiance and irradiance of the fluorescence (Hong et al., 2014). We prepared a ZnS:Cu phosphor layer through physical sediment method, and glass slides were washed with absolute ethyl alcohol. ZnS:Cu phosphors is about 10^{-2} mol% activator concentration and the grain size of the phosphor powder is 7.4 μm. Phosphor powder was mixed with acetone, and the mixture was poured into a plastic cup containing the glass slides and barium nitrate solution. After a specific period, the slides were removed from the plastic cup and then baked at 250 °C for 30 min. The thickness and density of ZnS:Cu phosphor layer are 65.38 μm and 1.635 g cm^{-3}. The ZnS:Cu phosphor layer was placed near the GaAs photovoltaic cell, which was fabricated by Shenzhen Yin-XuanSheng Technology Co., Ltd. The ^{147}Pm source (in the form of Pm_2O_3) with a density of activity of 2.9 mCi cm^{-2} was loaded on the phosphor layer, as shown in Fig. 2. The actual size of the nuclear battery is 1 cm × 1 cm.

2.2. Performance test

With ^{147}Pm excitation, the relative spectral irradiance of the fluorescence $I(\lambda)$ from the surface of ZnS:Cu phosphor layer was tested with a Cary Eclipse luminescence spectrophotometer (Agilent Technologies, USA), as shown in Fig. 3. The nuclear battery was placed in a high–low temperature test chamber to adjust the temperature. Current–Voltage (I–V) characteristics were obtained with a dual-channel system source meter instrument (Model 2636A, Keithley, USA).

3. Results and discussion

The electrical performance was measured within the temperature range of 223.15 K to 323.15 K. The I–V characteristics and electrical performance of the radioluminescent nuclear battery with the temperature are shown in Figs. 4 and 5. The two figures illustrate that the short-circuit current density (J_{sc}) slightly decreases with the increase in temperature, whereas V_{oc} and rapidly decrease.

3.1. Short-circuit current density J_{sc}

The p–n junction of the semiconductor absorbs the fluorescence, and the electron–hole pairs are produced within the space-charge and charge-neutral regions. According to the photovoltaic effect and the process of carrier generation, J_{sc} can be presented for the GaAs photovoltaic cell as follows (Nelson, 2003):

$$\begin{aligned} J_{sc} \approx & \int_0^{\infty} \{1 - \exp[-\alpha(x_p - w_p)]\}\left(1 + \frac{S_n}{\alpha D_n}\right) \\ & \times q(1-R)b_s(E)dE \\ & + \int_0^{\infty} \exp[-\alpha(x_p + w_n)] \\ & \{1 - \exp[-\alpha(x_n - w_n)]\}\left(1 - \frac{S_p}{\alpha D_p}\right)q(1-R)\,' \\ & \times b_s(E)dE \\ & + \int_0^{\infty} q(1-R)\exp[-\alpha(x_p - w_p)] \\ & \times\{1 - \exp[-\alpha(w_p + w_n)]\}b_s(E)dE \end{aligned} \quad (1)$$

where α is the absorption coefficient, x_p is the thickness of the p-type emitter, x_n is the thickness of n-type base, w_n is the n-type depletion width, w_p is the p-type depletion width, D_n is the electron diffusion constant, D_p is the hole diffusion constant, S_n is the electron surface recombination velocity, S_p is the hole surface recombination, q is the elementary charge, R is the reflectivity (Aspnes and Studna, 1983), and $b_s(E)$ is the spectral photon-flux density of the fluorescence. The relationship between α and photon energy (E) is shown as follows (Pankove, 1971):

$$\alpha(E) = \begin{cases} A(E - E_g)^{0.5} & E \geq E_g \\ 0 & E < E_g \end{cases}, \quad (2)$$

where A is a constant and E_g is the bandgap of the GaAs semiconductor. A is calculated as 2.4254×10^4 cm^{-1}. E_g and

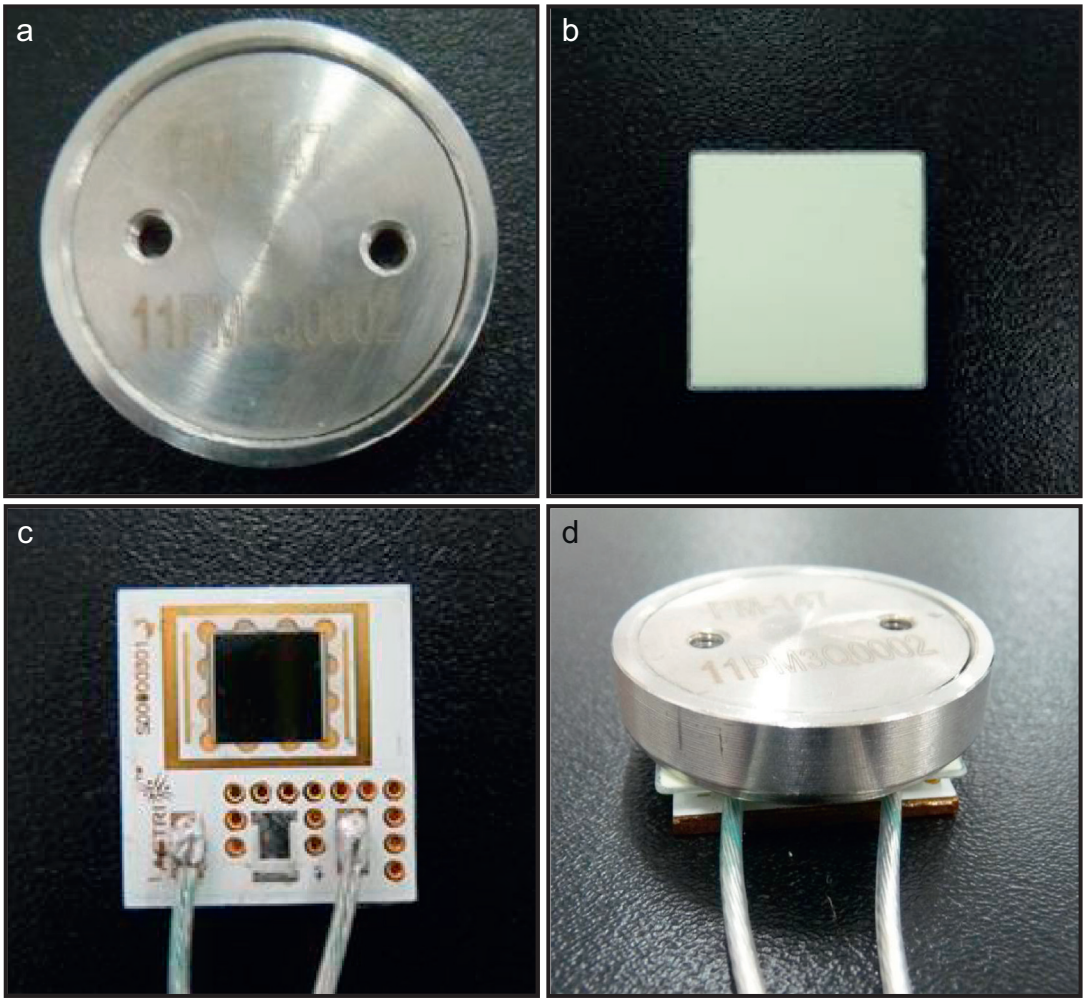

Fig. 2. (a) ^{147}Pm source, (b) ZnS:Cu phosphor layer, (c) GaAs photovoltaic cell, and (d) battery prototype setup.

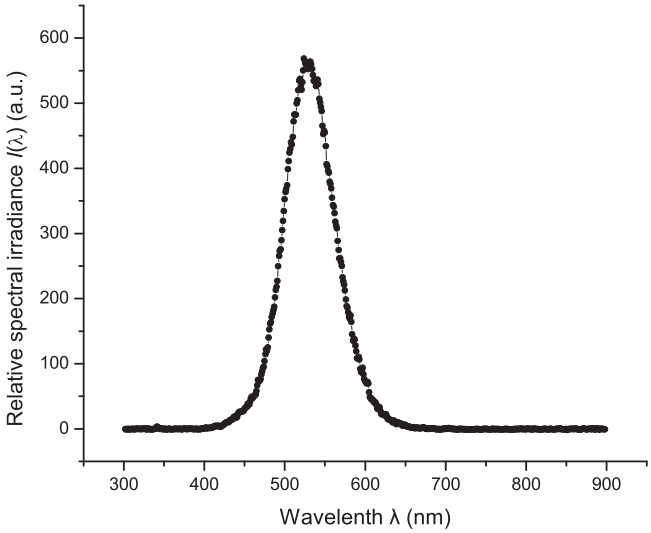

Fig. 3. Relative spectral irradiance of the ZnS:Cu phosphor layer.

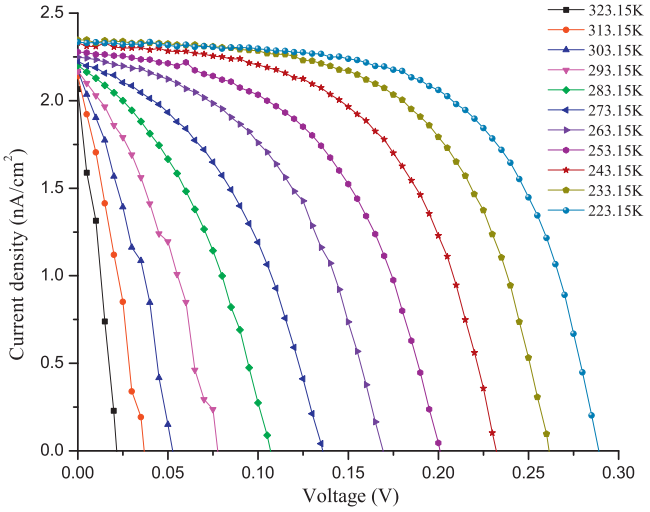

Fig. 4. *I–V* characteristic curves.

temperature T should satisfy the following equation:

$$E_g(T) = 1.519 - 5.405 \times 10^{-4}\frac{T^2}{(T+204)}. \quad (3)$$

x_p, x_n, are not affected by temperature. D_n, D_p, S_p, and S_n are hardly affected by temperature, and are considered as constants. The values of these parameters are listed in Table 1. The expressions of w_p and w_n are shown as follows (Nelson, 2003):

$$w_p = \frac{1}{N_a}\sqrt{\frac{2\varepsilon_0\varepsilon_s V_{bi}}{q((1/N_a)+(1/N_d))}}, \quad (4)$$

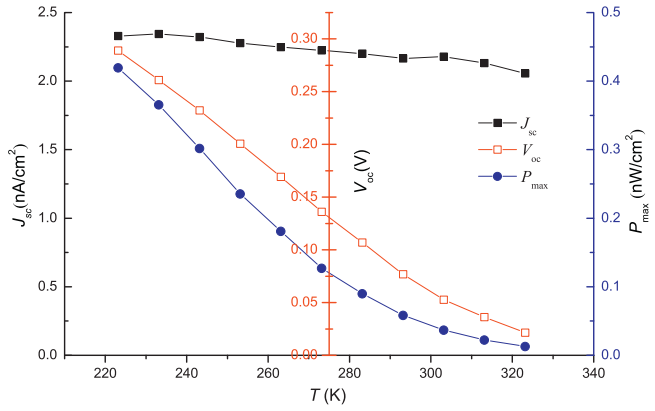

Fig. 5. Short-circuit current density J_{sc}, open-circuit voltage V_{oc} and maximum output power density P_{max} of the battery with the temperature.

$$w_n = \frac{1}{N_d}\sqrt{\frac{2\varepsilon_s\varepsilon_0 V_{bi}}{q((1/N_a)+(1/N_d))}}, \tag{5}$$

where N_a is the density of acceptor impurity atoms, N_d is the density of donor impurity atoms, ε_0 is the vacuum permittivity, ε_s is the GaAs semiconductor permittivity, and V_{bi} is the built-in voltage. The values of N_a and N_d are listed in Table 1. Moreover, ε_s and V_{bi} are expressed as follows (Nelson, 2003):

$$\varepsilon_s = 12.426 + 1.58\times 10^{-3}T, \tag{6}$$

$$V_{bi} = \frac{k_B T}{q}\ln\left(\frac{N_a N_d}{n_i^2}\right), \tag{7}$$

where n_i is the intrinsic carrier density and can be calculated using the following equation (Augustin et al., 2003):

$$n_i = \sqrt{N_c N_v}\cdot\exp\left(-\frac{E_g}{2k_B T}\right), \tag{8}$$

where N_c and N_v are the effective densities of state of the electrons in the conduction band and holes in valence band, which are equal to $4.7\times 10^{17}(T/300)^{3/2}$ and $7\times 10^{18}(T/300)^{3/2}$, respectively.

The value of $b_s(E)$ is obtained using Eq. (9).

$$b_s(E) = b_s\left(\frac{hc}{\lambda}\right) = \frac{\lambda^3}{(hc)^2}I(\lambda). \tag{9}$$

The energy efficiency of radiaoluminescence of ZnS:Cu phosphor layer under irradiation is related to the temperature. Namely, the temperature would affect the irradiance of ZnS:Cu phosphor layer. The instability of energy efficiency of radioluminescence of ZnS:Cu phosphors caused by temperature variations can be characterized by the coefficient K_T (Mikhal'chenko, 2003)

$$K_T = \frac{(\eta_{RL})_{T1}-(\eta_{RL})_{T2}}{(\eta_{RL})_{T1}(T_1-T_2)}\times 100 = (0.04\text{–}0.06)\%/K, \tag{10}$$

where, $(\eta_{RL})_{T1}$ and $(\eta_{RL})_{T2}$ are the energy efficiency at temperature T_1 and T_2. As shown in Eq. (10), the temperature hardly change the irradiance in the temperature range of 223.15 K to 323.15 K. The spectrum (spectral irradiance) of ZnS:Cu phosphors would shift to the short-wave direction as the temperature decrease, which is called the blue shift. Kallmann (1962) has studied the temperature dependence on spectrum of ZnS:Cu phosphors. From the result of Kallmann' reserch, the influence of temperature on ZnS:Cu spectrum is very little. Thus, $b_s(E)$ remains nearly constant within the temperature range of 223.15 K to 323.15 K.

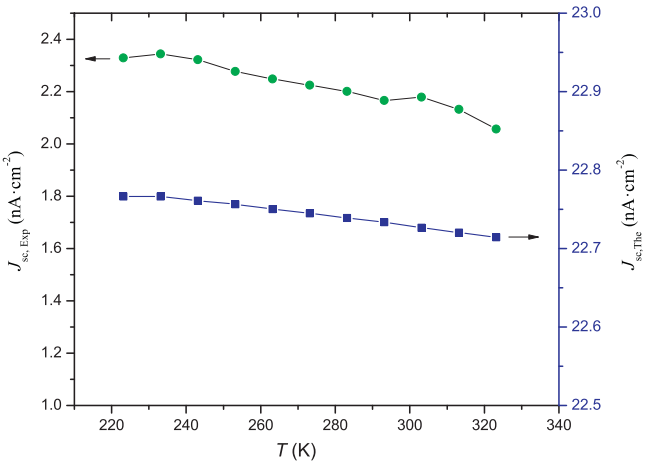

Fig. 6. Theoretical and experimental relationships between short-circuit current density and temperature.

Refer to the method introduced in reference Hong et al. (2014), the calculated value of spectral photon-flux density $b_{s,cal}(E)$ can be obtained. According to Eq. (1), the trend of theoretical value of short-circuit current density $J_{sc,The}$ are presented in Fig. 6. From the Fig. 6, $J_{sc,The}$ exceeds by about one order the value of experiment $J_{sc,Exp}$, the most likely reason is that we described the ^{147}Pm source with a purity of 100% in the theoretical calculation, while the ^{147}Pm source utilized in the experiment contains abundant gold or silver powder and which absorb a large amount of energy. Athough the values of both are different, the two plots all slightly decrease with the increase in temperature.

Some studies in the literature proposed that J_{sc} minimally increases with the increasing temperature for photovoltaic cells under sunlight irradiation; this result contradicts our conclusion. The main reason for the discrepancy could be attributed to the wide solar spectrum range and the ability of the photovoltaic cells to absorb more photons as indicated by the decrease in E_g with the increasing temperature (see Eq. (3)). However, the spectral irradiance of fluorescence (see Fig. 3) is narrow, and the energy of photons is higher than E_g; thus, the absorption of photons by the photovoltaic cells cannot be gained with increase of the temperature. Moreover, the changes in α, w_p, w_n, and E_g can result in the gradual decrease of J_{sc}.

3.2. Open-circuit voltage V_{oc}

A photovoltaic cell can be generally characterized using the equivalent circuit of a diode model as presented in Fig. 7, where I_{ph}, R_s, and R_{sh} are the photocurrent, series resistance, and shunt resistance, respectively. In an ideal situation, R_s is assumed to be equal to zero and R_{sh} is infinitely high. Therefore, V_{oc} of the equivalent circuit is shown as follows:

Table 1
Parameters of the GaAs photovoltaic cell.

x_p (μm)	x_n (μm)	D_n (cm^2 s^{-1})	D_p (cm^2 s^{-1})	S_p (cm s^{-1})	S_n (cm s^{-1})	N_a (10^{18} cm^{-3})	N_d (10^{17} cm^{-3})
0.2	4	25	100	1,000	1,000	3.5	2

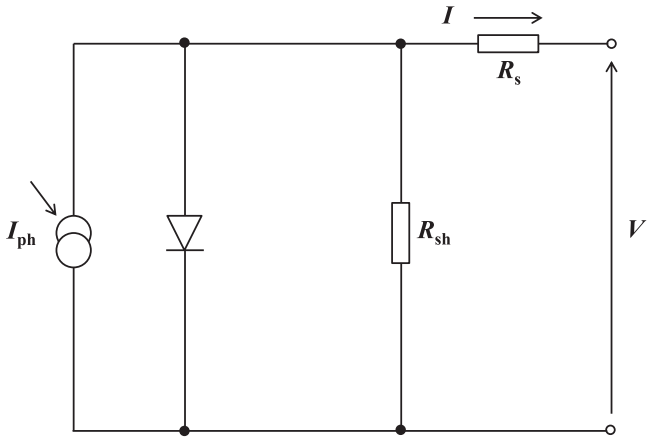

Fig. 7. Equivalent circuit of a photovoltaic cell.

$$V_{oc} = \frac{nkT}{q} \ln (J_{sc}/J_0), \tag{11}$$

where n and J_0 are the ideality factor and the reverse-saturation current density, respectively. For the GaAs photovoltaic cell, n is equal to 2, and J_0 is given by

$$J_0 = \frac{qn_i(w_n + w_p)}{\sqrt{\tau_n \tau_p}}. \tag{12}$$

where t_n and t_p are the electron and hole lifetimes, respectively. Moreover, n_i rapidly increases with the increase in temperature (see Eq. (8)), whereas the sensitivities of w_n, w_p, t_n, and t_p on temperature are low. Thus, these parameters (w_n, w_p, t_n, and t_p) can be considered constants. The dark current (J_{dark}) of the photovoltaic cell can be expressed as follows:

$$J_{dark} = J_0\left[exp\left(\frac{qV}{2k_BT}\right)\right]. \tag{13}$$

Eq. (13) can be converted into Eq. (14). Hence,

$$\ln J_{dark} = \frac{q}{2kT}\cdot V + \ln J_0. \tag{14}$$

The relationship between J_{dark} and V of the GaAs photovoltaic cell under the temperature of 300 K was measured with a dual-channel system source meter instrument in the dark (without the ZnS:Cu phosphor layer or ^{147}Pm source). The curve of $\ln J_{dark}$ with regard to V is shown in Fig. 8. After the linear fitting of the curve, the vertical intercept of the fitted straight line is the value of $\ln J_0$ under 300 K. Thus, $J_0(T)$ can be simplified as Eq. (15) according to Fig. 8 and Eq. (12):

$$J_0(T) = 3.54687 \times 10^{-17} n_i. \tag{15}$$

According to Eqs. (8), (11), and (15), the temperature coefficient (dV_{oc}/dT) of V_{oc} can be calculated by

$$\frac{dV_{oc}}{dT} = \frac{2k}{q} \ln\left(\frac{J_{sc}}{3.54687 \times 10^{-17}}\right) - \frac{k}{q} \ln\left(\frac{4.7 \times 10^{17}}{300^{3/2}} \times \frac{7 \times 10^{18}}{300^{3/2}}\right) - \frac{3k}{q}(1 + \ln T). \tag{16}$$

As shown in Eq. (16), the change of dV_{oc}/dT is very small, and the value is negative after substituting the parameters. Thus, V_{oc} linearly decreases with the increase in temperature. According to Eqs. (8), (11), and (15) and by substituting the experimental value of J_{sc} (2.2 nA cm^{-2}), the theoretical values of V_{oc} can be obtained as a function of temperature as shown in Fig. 9. The experimental

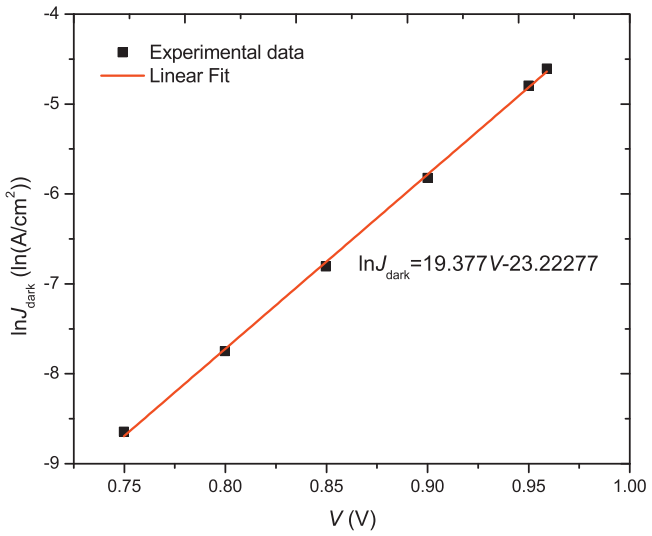

Fig. 8. J–V characteristics in the dark.

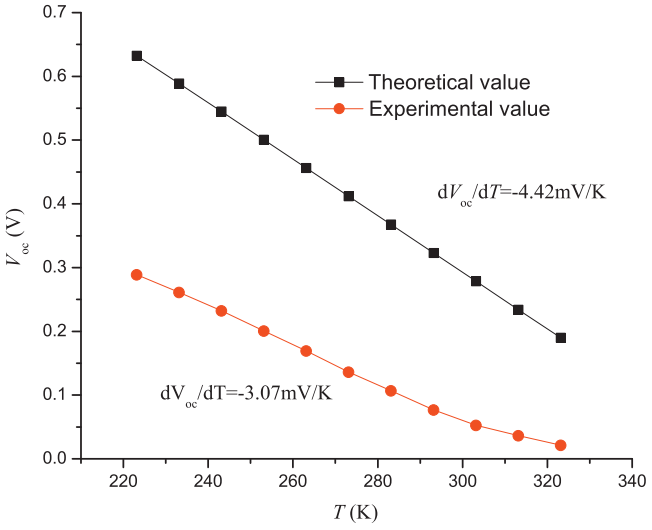

Fig. 9. Theoretical and experimental relationships between open-circuit voltage and temperature.

values of V_{oc} are also shown in Fig. 9. After the linear fitting, the experimental and theoretical values of dV_{oc}/dT are −3.07 and −4.42 mV/K, respectively, within the low-temperature region (223.15–293.15 K). The values of V_{oc} and dV_{oc}/dT differ between the theoretical and theoretical values. The difference is the exclusion of R_s and R_{sh} in the calculation, which both change with the temperature. The partial pressure of R_s results in lower V_{oc} experimental values than the theoretical values; hence, R_{sh} produces low dV_{oc}/dT because of the leaking current.

3.3. Maximum output power density P_{max} and total energy conversion efficiency η_T

The maximum power outputs of the nuclear battery under different temperatures are shown in Fig. 10. As shown in the figure, P_{max} is significantly related to temperature. P_{max} is elevated by 7 times when the temperature is reduced from the room temperature (293.15 K) to 223.15 K but decreases to a quarter of the original P_{max} when the temperature reaches 323.15 K. Therefore, the operating temperature of the nuclear cells should be considered when battery power is selected for practical applications.

The total energy conversion efficiency of the battery η_T can be

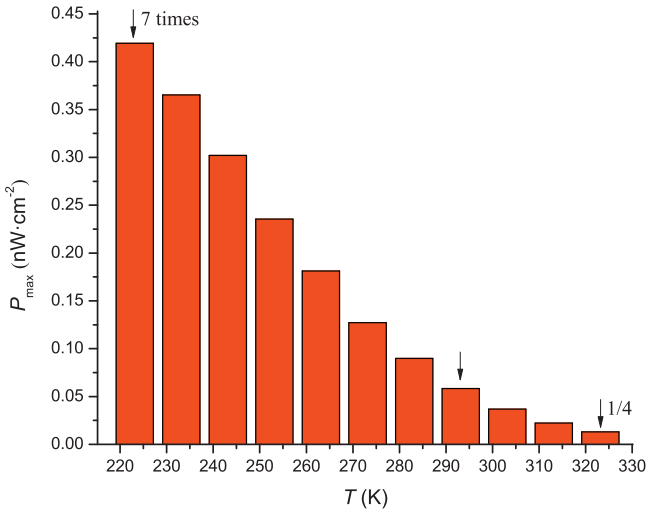

Fig. 10. Relationship of maximum output power density and temperature.

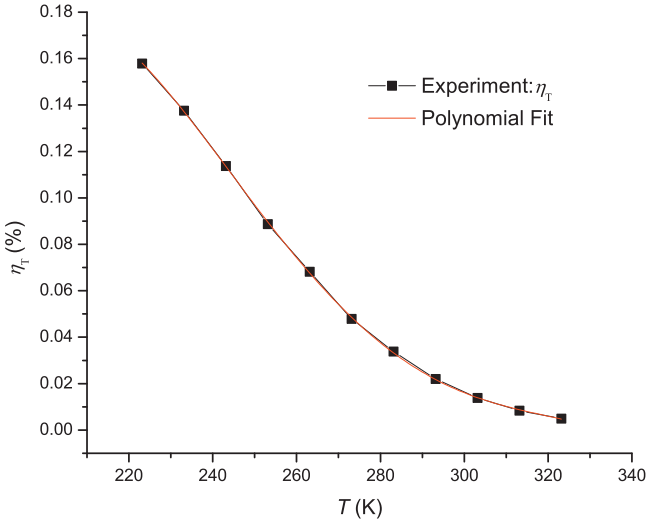

Fig. 11. Temperature T dependences of η_T.

calculated by

$$\eta_T = \frac{P_{max}}{AE_\beta} \quad (17)$$

where A is the ^{147}Pm radioisotope activity, and E_β is the average beta energy of 62 keV for ^{147}Pm radioisotope. Fig. 11 shows that η_T is highly sensitive to temperature. After polynomial fitting, η_T exhibit a four-parameter polynomial function dependence, as shown in Eq. (18).

$$\eta_T = -0.12621 + 0.00195T - 1.08819 \times 10^{-5}T^2 + 2.62465 \times 10^{-8}T^3 - 2.33119 \times 10^{-11}T^4 \quad (18)$$

4. Conclusion

The ZnS:Cu phosphor layer was fabricated using physical sediment method, and the ^{147}Pm source was loaded to form an illuminated light source. The light source was assembled with the GaAs photovoltaic cell to constitute a radioluminescent nuclear battery. A high–low temperature test chamber was used to adjust the temperature of the nuclear battery from 223.15 K to 323.15 K. The electrical performance of the nuclear battery was then measured. J_{sc} slightly decreases with the increasing temperature, whereas V_{oc} rapidly decreases. The value of dV_{oc}/dT is -3.07 mV/K within the low-temperature range of 223.15 K to 303.15 K. The effect of temperature on the output battery performance is mainly attributed to the sensitivity of the GaAs photovoltaic cell. Semiconductor parameters such as E_g, w_n, w_p, and n_i also change with the temperature.

P_{max} is significantly affected by temperature, in which P_{max} significantly increases with the increase in the temperature. The nuclear battery may not function under high-temperature condition but effectively performs under low temperature. The linear and significant dV_{oc}/dT may generate a temperature transducer with long service time from the nuclear battery. Repeatability tests should be conducted under high- and low-temperature conditions to obtain accurate and reliable transducer results.

The total energy conversion efficiency of the battery (η_T) in the experiment is very small. Several factors restrict η_T, such as self-absorption of source for β particle and ZnS:Cu phosphor layer for fluorescence. The ^{147}Pm source was prepared through powder metallurgy method (Raybould et al., 1979) and the active block of ^{147}Pm contains abundant gold or silver powder and is sealed in a stainless steel shell. The ZnS:Cu phosphor layer is non-transparent and the absorption of fluorescence is considerable. So materials is needed to improve for increasing η_T.

Acknowledgments

Supported by the National Natural Science Foundation of China (Grant no. 11205088), the Aeronautical Science Foundation of China (Grant no. 2012ZB52021), the Natural Science Foundation of Jiangsu Province (Grant no. BK20141406), the Funding of Jiangsu Innovation Program for Graduate Education (Grant no. CXZZ12_0146) and the Fundamental Research Funds for the Central Universities, and the Priority Academic Program Development of Jiangsu Higher Education Institutions. Liang Hong contributed equally to this work and should be considered co-first author.

References

Aspnes, D.E., Studna, A.A., 1983. Dielectric functions and optical parameters of Si, Ge, GaP, GaAs, GaSb, InP, InAs, and InSb from 1.5 to 6.0 eV. Phys. Rev. B 27 (2), 985–1009.
Augustin, M., Tom, M., Luis, C., 2003. Practical Handbook of Photovoltaics: Fundamentals and Applications. Elsevier.
Bower, K.E., Barbanel, Y.A., Shreter, Y.G., et al., 2002. Polymers, phosphors, and voltaics for radioisotope microbatteries. Boca Raton, London, New York, Washington, D.C..
Brown, P.M., 2008. Solid state radioisotopic energy converter for space nuclear power. In: Proceedings of the tenth symposium on space nuclear power and propulsion. 271(1), pp. 325–331.
Cress, C.D., Redino, C.S., Landi, B.J., et al., 2008. Alpha-particle-induced luminescence of rare-earth-doped Y_2O_3 nanophosphors. J. Solid. State. Chem. 181 (8), 2041–2045. http://dx.doi.org/10.1016/j.jssc.2008.04.024.
Chandrashekhar, M.V.S., Duggirala, R., Spencer, M.G., et al., 2007. 4*H* SiC betavoltaic powered temperature transducer. Appl. Phys. Lett. 91 (5), 053511–053511-3. http://dx.doi.org/10.1063/1.2767780.
Hong, L., Tang, X.B., Xu, Z.H., et al., 2014. Radioluminescent nuclear batteries with different phosphor layers. Nucl. Instrum. Meth. B 338, 112–118. http://dx.doi.org/10.1016/j.nimb.2014.08.005.
Hong, L., Tang, X.B., Xu, Z.H., et al., 2014. Parameter optimization and experment verification for a beta radioluminescence nuclear battery. J. Radioanal. Nucl. Chem. 302 (1), 701–707. http://dx.doi.org/10.1007/s10967-014-3271-2.
Kallmann, H.P., (editor) 1962. Luminescence of Organic and Inorganic Materials. 229-630.
Liu, Y.P., Tang, X.B., Xu, Z.H., et al., 2014. Optimization and temperature effects on sandwich betavoltaic microbattery. Sci. China Technol. Sci. 57 (1), 14–18. http://dx.doi.org/10.1007/s11431-013-5413-0.
Mikhal'chenko, G.A., 2003. Radioluminescent Emitters. Energoatomizdat, Moscow. [Russian language].
Nelson, J., 2003. The Physics of Solar Cells. Imperial college press, London.
Prelas, M.A., Charlson, E.J., Charlson, E.M., et al., 1993. Diamond photovoltaic in

energy conversion. In: Proceedings of the Second International Conference on the Application of Diamond Films and Related Materials.
Prelas, M.A., Popovici, G., Khasawinah, S., et a., 1995. In: Prelas M.A., Gielisse P., Popovici G., Spitsyn B.V., Stacy T. (ed.), Wide band-gap photovoltaics. Springer, Netherlands, 463–474.
Prelas, M.A., Weaver, M.L., Watermann, E.D., et al., 2014. A review of nuclear batteries. Prog. Nucl. Energ. 75, 117–148, http://dx.doi.org/10.1016/j.pnucene.2014.04.007.
Pankove, J.I., 1971. Optical Processes in Semiconductors. Dover Publications, New York.
Qiao, D.Y., Chen, X.J., Ren, Y., et al., 2011. A micro nuclear battery based on sic schottky barrier diode. J. Microelectromech. S 20 (3), 685–690. http://dx.doi.org/10.1109/JMEMS.2011.2127448.
Raybould, D., Morris, D.G., Cooper, G.A., 1979. A new powder metallurgy method. J. Mater. Sci. 14 (10), 2523–2526. http://dx.doi.org/10.1007/BF00737047.
Sychov, M., Kavetsky, A., Yakubova, G., et al., 2008. Alpha indirect conversion radioisotope power source. Appl. Radiat. Isot. 66 (2), 173–177. http://dx.doi.org/10.1016/j.apradiso.2007.09.004.
Sims, P.E., Dinetta, L.C., Barnett, A.M., 1994. High efficiency GaP power conversion for Betavoltaic applications. In: Proceedings of the 13th Space Photovoltaic Research and Technology Conference. 1, pp. 373–382.
Walko, R.J., Ashley, C.S., Brinker, C.J., et al., 1990. Electronic and photonic power applications. In: Proceedings of the Radioluminescent Lighting Technology Transfer Conference.
Wang, G.Q., Hu, R., Wei, H.Y., et al., 2010. The effect of temperature changes on electrical performance of the betavoltaic cell. Appl. Radiat. Isot. 68 (12), 2214–2217. http://dx.doi.org/10.1016/j.apradiso.2010.06.011.